Ultrasonic Data Compression via Parameter Estimation

Guilherme Cardoso and Jafar Saniie, *Senior Member, IEEE*

***Abstract*—Ultrasonic imaging in medical and industrial applications often requires a large amount of data collection. Consequently, it is desirable to use data compression techniques to reduce data and to facilitate the analysis and remote access of ultrasonic information. The precise data representation is paramount to the accurate analysis of the shape, size, and orientation of ultrasonic reflectors, as well as to the determination of the properties of the propagation path. In this study, a successive parameter estimation algorithm based on a modified version of the continuous wavelet transform (CWT) to compress and denoise ultrasonic signals is presented. It has been shown analytically that the CWT (i.e., time × frequency representation) yields an exact solution for the time-of-arrival and a biased solution for the center frequency. Consequently, a modified CWT (MCWT) based on the Gabor-Helstrom transform is introduced as a means to exactly estimate both time-of-arrival and center frequency of ultrasonic echoes. Furthermore, the MCWT also has been used to generate a phase × bandwidth representation of the ultrasonic echo. This representation allows the exact estimation of the phase and the bandwidth. The performance of this algorithm for data compression and signal analysis is studied using simulated and experimental ultrasonic signals. The successive parameter estimation algorithm achieves a data compression ratio of (1–5N/J), where J is the number of samples and N is the number of echoes in the signal. For a signal with 10 echoes and 2048 samples, a compression ratio of 96% is achieved with a signal-to-noise ratio (SNR) improvement above 20 dB. Furthermore, this algorithm performs robustly, yields accurate echo estimation, and results in SNR enhancements ranging from 10 to 60 dB for composite signals having SNR as low as −10 dB.**

I. Introduction

Signal modeling and parameter estimation for detecting and estimating multiple interfering echoes has been the subject of study in the field of ultrasonic imaging over the past two decades. In particular, Saniie [1] and Saniie *et al.* [2], [3] have dealt with the ultrasonic signal analysis and modeling for nondestructive evaluation (NDE) applications when targets are reverberant and/or randomly distributed. In medical imaging, a large number of papers have dealt with modeling of ultrasonic signals and obtaining parameters for mean scatterer spacing and tissue characterization (e.g., [4]–[12]). Modeling of superimposed signals and parameter estimation also have been studied by Feder and Weinstein [13]. More recently, the modeling and estimation of the ultrasonic signal parameters using the maximum likelihood estimation and the expectation maximization algorithm have been introduced by Demirli and Saniie [14], [15].

In this study, we present a successive parameter estimation algorithm that relies on the assumption that any ultrasonic signal, no matter how complex it is, can be decomposed into the superposition of multiple, single Gaussian echoes. The goal is to efficiently estimate the parameters of the individual echoes. Most importantly, with ultrasonic signal parameters, we can establish the analytical relationship between the signal model and the physical parameters of materials.

The continuous wavelet transform (CWT) is an effective method to display the time × frequency (TF) information of signals, and it has been used for flaw detection in ultrasonic applications [16] and [17]. In particular, the Morlet wavelet [18] is used to successively estimate the echo parameters (amplitude, bandwidth, phase, time-of-arrival, and center frequency). In this paper, it is shown analytically that the CWT (i.e., time × frequency representation) yields an exact solution for the time-of-arrival and a biased estimation of the center frequency. Consequently, a modified CWT (MCWT), based on the Gabor-Helstrom transform, is introduced as a means to exactly estimate both time-of-arrival and center frequency of ultrasonic echoes. The parameter estimation method presented in this paper uses the MCWT to perform the correlation of a mother wavelet with the ultrasonic signal [19] and [20]. Because this is a successive approach, the parameter estimation algorithm keeps searching until the estimation satisfies the error criteria. The error criteria can be generated based on the maximum number of echoes, the minimum echo energy, and/or the position of echoes. The parameters of the ultrasonic echo have different physical significance. Furthermore, the error in the estimation of each of the parameters affects the overall estimation accuracy differently. Thus, we have analyzed the sensitivity of the reconstruction error to the disparity of the estimated parameters.

The successive parameter estimation algorithm presented in this paper has several advantages over discrete time lossy compression techniques such as JPEG [21] and SPIHT [22]. Most data compression algorithms offer a compromise between compression ratio and signal fidelity [23]–[25]. Furthermore, discrete time techniques are not suitable for the estimation of the ultrasonic signal parameters (i.e., bandwidth, amplitude, center frequency, phase,

Manuscript received December 27, 2003; accepted September 15, 2004.

The authors are with the Department of Electrical and Computer Engineering, Illinois Institute of Technology, Chicago, Illinois 60616 (e-mail: sansonic@ece.iit.edu).

and time-of-arrival). Therefore, in both medical and industrial imaging applications, a well-defined modeling of the ultrasonic echoes leading to the accurate parameter estimation is highly desirable for target detection, deconvolution, object classification, velocity measurement, and ranging system.

II. Successive Parameter Estimation Algorithm

The ultrasonic signal can be represented as a superposition of Gaussian echoes [14]. In pulse-echo ultrasonic testing, the backscattered echo from a single reflector can be modeled as:

$$f_\Theta(t) = \beta \exp\left[-\alpha(t-\tau)^2\right] \cos\left(2\pi f_c(t-\tau) + \phi\right), \tag{1}$$

where $\Theta = [\alpha, \beta, f_c, \phi, \tau]$ denotes the parameter vector. The parameters of this model are closely related to the physical properties of the ultrasonic signal propagating through the material. The time-of-arrival, τ, is related to the distance between the transducer and the reflector. The amplitude, β, is a function of the attenuation of the original signal and the size of the reflector relative to the beam field. The amplitude of the reflected signal also depends on the size of the reflector or scatterer compared with the wavelength. The parameters f_c and α are the center frequency and bandwidth factor, respectively. These parameters are governed by the transducer frequency characteristics and the propagation path. The phase of the signal, ϕ, accounts for the distance, impedance, size, and orientation of the reflector [26].

The first step in building the parameter estimation algorithm is to identify the behavior of the signal parameters and the influence they have in the reconstruction error of the signal. Thus we examined the reconstruction error as each of the parameters is altered. This simulates the situation in which all the parameters, with the exception of one, are correctly estimated. The reconstruction error, E_r, is calculated as:

$$E_r = \left\| f_\Theta(t) - f_{\hat{\Theta}}(r) \right\|, \tag{2}$$

where $\hat{\Theta}$ is the vector of estimated parameters. Fig. 1 shows how E_r behaves as each of the estimated parameters deviates from -10% to 10% of its actual value. Fig. 1 reveals that the reconstruction error is more sensitive to time-of-arrival, τ, compared to other parameters. Hence, τ is the most critical parameter to be estimated, followed by f_c, β, ϕ, and α (i.e., successive parameter estimation algorithm).

The successive parameter estimation algorithm is a recursive method that starts with a TF representation (MCWT) of the input signal. The successive estimation is achieved by applying a window to the TF representation in order to separate interfering echoes. The window process removes part of the echo's energy that overlaps with neighboring echoes; therefore, it creates an incomplete echo. These windows are centered on each MCWT peak, and their size is determined by the proximity of the nearby echoes. Therefore, the parameter estimation algorithm relies on the detection of the ultrasonic echoes in the TF representation of the ultrasonic signal. The peaks of the TF representation provide information about the time-of-arrival and frequency of the multiple echoes embedded in the ultrasonic signal. Upon detection of a peak, an automatic windowing procedure is used to separate adjacent and interfering echoes. The window design strategy used to separate the ultrasonic echoes depends on the noise embedded on the signal. When the signal-to-noise ratio (SNR) is high, the window procedure separates neighbor echoes using their respective projections in the time and frequency domains. If the SNR is low, it is desirable to constrain the window to a smaller region around the TF representation peak that represents the best SNR of the echo. The window must be small to minimize the introduction of noise in the estimation, but it must be large enough to contain sufficient information about the echo.

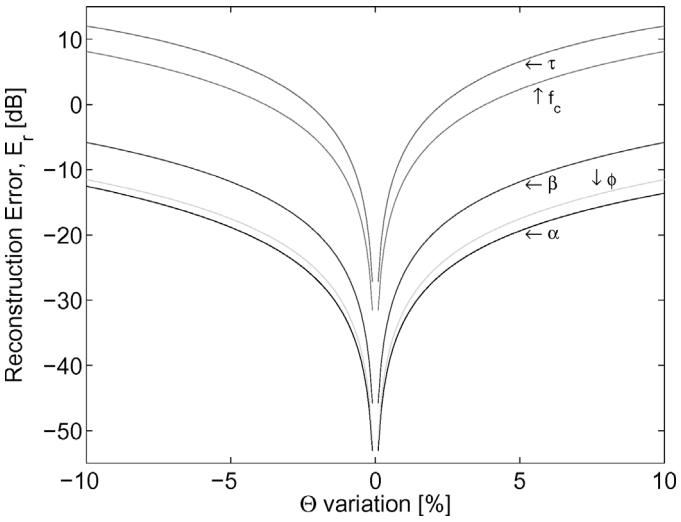

Fig. 1. Effect of uncertainty of the values of parameters on reconstruction error, E_r.

A. Echo Parameter Estimation Algorithms

The CWT of $f_\Theta(t)$ with respect to a wavelet kernel $\psi(t)$ is defined as [27]:

$$CWT(a,b) = \int_{t=-\infty}^{\infty} f_\Theta(t)\psi^*_{a,b}(t)dt. \tag{3}$$

The variable b represents time shifts in the wavelet kernel, and a is a positive variable and is referred to as the scale of the dilation. The CWT maps $f_\Theta(t)$ into a two-dimensional TF representation. The inverse CWT is defined as:

$$f_\Theta(t) = \frac{1}{c} \int_{a=-\infty}^{\infty} \int_{b=-\infty}^{\infty} \frac{1}{a^2} CWT(a,b)\psi_{a,b}(t)dbda, \tag{4}$$

where c is a scaling constant that satisfies the wavelet's admissibility condition [27] and:

$$\psi_{a,b}(t) = \frac{1}{\sqrt{a}}\psi\left(\frac{t-b}{a}\right). \tag{5}$$

The distance between $f_\Theta(t)$ and $\psi_{a,b}(t)$ is the norm of the difference of the two signals:

$$\begin{aligned}&\|f_\Theta(t) - \psi_{a,b}(t)\|^2 = \\ &\|f_\Theta(t)\|^2 + \|\psi_{a,b}(t)\|^2 - 2\,\mathrm{Re}[CWT(a,b)].\end{aligned} \tag{6}$$

Minimizing $\|f_\Theta(t) - \psi_{a,b}(t)\|^2$ in terms of variables a and b will provide the best similarity between $f_\Theta(t)$ and $\psi_{a,b}(t)$. The quantities $\|f_\Theta(t)\|^2$ and $\|\psi_{a,b}(t)\|^2$ on the right-hand side of (6) are positive constants that are independent of a and b. Hence, the minimization of $\|f_\Theta(t) - \psi_{a,b}(t)\|^2$ implies the maximization of $\mathrm{Re}[CWT(a,b)]$. Furthermore, $\|f_\Theta(t) + \psi_{a,b}(t)\|^2$ also measures the similarity between the echo, $f_\Theta(t)$, and the wavelet, $-\psi_{a,b}(t)$. This similarity implies that the minimum of $\mathrm{Re}[CWT(a,b)]$ also represents the closeness between the ultrasonic echo and the wavelet. Therefore, the maximum of the absolute value of $\mathrm{Re}[CWT(a,b)]$, $abs\,\{\mathrm{Re}[CWT(a,b)]\}$, in terms of variables a and b represents the point of best similarity between the signal $f_\Theta(t)$ and the wavelet kernel $\psi_{a,b}(t)$ or $-\psi_{a,b}(t)$.

The Morlet [20] is the wavelet kernel of choice due to its similarity to the echoes, and that brings many advantages in the decomposition of ultrasonic signals [16], [17], and [28]. The Morlet wavelet is defined as:

$$\psi_{a,b}(t) = \frac{1}{\sqrt{a}}\exp\left[-\gamma_0\left(\frac{t-b}{a}\right)^2 + i\omega_0\left(\frac{t-b}{a}\right)\right], \tag{7}$$

where the variable a tracks the frequency and the variable b tracks the time-of-arrival of the echo, ω_0 and γ_0 are the center frequency and bandwidth factor of the Morlet wavelet kernel, respectively. The term $\frac{1}{\sqrt{a}}$ ensures that the energy of the wavelet kernel is the same for all a and b. The Morlet wavelet kernel is a complex function and it is one sided in the frequency domain. Hence, the CWT of the ultrasonic echo shown in (1) is equivalent to the CWT of the ultrasonic echo represented as $\beta\exp\left[-\alpha(t-\tau)^2 + i\left(2\pi f_c(t-\tau)+\phi\right)\right]$. Then, the $CWT(a,b)$ of a single ultrasonic echo becomes:

$$\begin{aligned}CWT(a,b) = \frac{\beta}{\sqrt{a}}\int_{t=-\infty}^{\infty}\exp\Bigg[&-t^2\left(\alpha+\frac{\gamma_0}{a^2}\right)\\ &-t\left(-2\alpha\tau - i\omega_c + \frac{2b\gamma_0}{a^2} + \frac{i\omega_0}{a}\right)\\ &-\left(\alpha\tau^2 + i\omega_c\tau - i\phi + \frac{\gamma_0 b^2}{a^2} - \frac{ib\omega_0}{a}\right)\Bigg]dt,\end{aligned} \tag{8}$$

where $\omega_c = 2\pi f_c$. The solution to (8) is simplified to (9) (see next page). The magnitude of the $CWT(a,b)$ is given by:

$$\begin{aligned}&|CWT(a,b)| = \\ &\beta\sqrt{\frac{a\pi}{\alpha a^2+\gamma_0}}\exp\left[\frac{-\left(\omega_c - \frac{\omega_0}{a}\right)^2 - \frac{4\gamma_0\alpha}{a^2}(b-\tau)^2}{4\left(\alpha+\frac{\gamma_0}{a^2}\right)}\right].\end{aligned} \tag{10}$$

The maximum of $|CWT(a,b)|$ in terms of a and b is the same as the maximum of $abs\{\mathrm{Re}[CWT(a,b)]\}$, because $abs\{\mathrm{Re}[CWT(a,b)]\}$ can be represented as:

$$abs\{\mathrm{Re}[CWT(a,b)]\} = |CWT(a,b)|abs\{\cos(g(\Theta))\}, \tag{11}$$

where $g(\Theta)$ is a function of the echo parameters. The term $|CWT(a,b)|$ in the right-hand side of the above equation does not depend on the phase of the echo, ϕ. The cosine term, on the contrary, depends on ϕ. Hence, this extra degree of freedom can be used to set the cosine term to unity, which yields that the maximum of $|CWT(a,b)|$ in terms of a and b is the same as the maximum of $abs\{\mathrm{Re}[CWT(a,b)]\}$. The maximization of $|CWT(a,b)|$ can be obtained by taking the partial derivatives of (11) with respect to variables b and a and setting the outcome to zero, giving (12) (see next page). The solution to (12) is $b=\tau$, which proves that the CWT peak is the exact estimation of the time-of-arrival. Furthermore (13) (see next page) implies that:

$$\left(a\frac{\left(-a\gamma_0\omega_c^2 - a^2\alpha\omega_c\omega_0 + \omega_0^2 a\alpha + \gamma_0\omega_c\omega_0\right)}{a^2\alpha+\gamma_0} + \left(\gamma_0 - a^2\alpha\right)\right) = 0. \tag{14}$$

The solution of (14) does not yield an exact estimation of the center frequency which is $\omega_c = \frac{\omega_0}{a}$. Hence, there is a bias in the estimation of the center frequency when using the CWT. To calculate the bias, it is considered that $\omega_c = \frac{\omega_0}{a} + \delta$, where δ is the estimation bias. Substituting this result into (14) leads to:

$$\delta^2\left(a^2\gamma_0\right) + \delta\left(\omega_0 a\gamma_0 + \omega_0 a^3\alpha\right) + a^4\alpha^2 - \gamma_0^2 = 0. \tag{15}$$

The explicit solution for the bias is (16) (see next page).

There are two possible solutions to (15), δ_+ and δ_-. In the case where $\gamma_0 = \alpha$ and $a = 1$ (i.e., $\omega_c = \omega_0$) (16) simplifies to (17) and (18) (see page 317).

Thus the correct solution for the center frequency bias is given by δ_+. Furthermore, the bias is unknown and cannot be used to correct the frequency estimation because the bandwidth factor and the phase are not known a priori.

To circumvent the biasness of the CWT, a modified version of the CWT (MCWT) has been developed. The MCWT is introduced as a means to exactly estimate all parameters of the ultrasonic echo. The estimation of the center frequency, time-of-arrival, bandwidth factor, phase, and amplitude is executed with an overcomplete Morlet wavelet kernel, $\psi_{\hat{\Theta}}(t)$, that spans in γ (bandwidth factor) and θ (phase) space:

$$\psi_{\hat{\Theta}}(t) = \frac{1}{\sqrt{\varepsilon}}\exp\left[-\gamma(t-b)^2 + i\omega_0\left(\frac{t-b}{a}\right) + i\theta\right], \tag{19}$$

$$CWT(a,b) = \beta\sqrt{\frac{a\pi}{\alpha a^2+\gamma_0}}\exp\left[\frac{-\left(\omega_c-\frac{\omega_0}{a}\right)^2-\frac{4\alpha\gamma_0}{a^2}(b-\tau)^2+i\left(4\left(\frac{\alpha\omega_0}{a}+\frac{\gamma_0\omega_c}{a^2}\right)(b-\tau)+4\phi\left(\alpha+\frac{\gamma_0}{a^2}\right)\right)}{4\left(\alpha+\frac{\gamma_0}{a^2}\right)}\right]. \quad (9)$$

$$\frac{\partial|CWT(a,b)|}{\partial b} = -\beta\sqrt{\frac{a\pi}{\alpha a^2+\gamma_0}}\exp\left[\frac{-\left(\omega_c-\frac{\omega_0}{a}\right)^2-\frac{4\gamma_0\alpha}{a^2}(b-\tau)^2}{4\left(\alpha+\frac{\gamma_0}{a^2}\right)}\right]\left(\frac{2\alpha\gamma_0(b-\tau)}{a^2\alpha+\gamma_0}\right)=0. \quad (12)$$

$$\frac{\partial|CWT(a,b)|^2}{\partial a} = \frac{\pi\beta^2}{\left(a^2\alpha+\gamma_0\right)^2}\exp\left[\frac{-\left(\omega_c-\frac{\omega_0}{a}\right)^2}{2\left(\alpha+\frac{\gamma_0}{a^2}\right)}\right]\left(\frac{a\left(-a\gamma_0\omega_c^2-a^2\alpha\omega_c\omega_0+\omega_0^2a\alpha+\gamma_0\omega_c\omega_0\right)}{a^2\alpha+\gamma_0}+\left(\gamma_0-a^2\alpha\right)\right)=0, \quad (13)$$

$$\delta_+,\,\delta_- = \frac{-\omega_0\left(a^2\alpha+\gamma_0\right)\pm\sqrt{\omega_0^2\left(a^4\alpha^2+2a^2\alpha\gamma_0+\gamma_0^2\right)-4\gamma_0\left(a^4\alpha^2-\gamma_0^2\right)}}{2a\gamma_0}. \quad (16)$$

where the term $\frac{1}{\sqrt{\varepsilon}}$ normalizes the energy of the modified wavelet kernel, and $\varepsilon = \sqrt{\frac{\pi}{2\gamma}}$. This overcomplete Morlet wavelet differs from the kernel used in the Gabor-Helstrom transform ([16] and [29]) by including two additional parameters: phase and bandwidth. The $\hat{\Theta} = \left[\gamma,\,\hat{\beta},\,\frac{\omega_0}{2\pi a},\,\theta,\,b\right]$ represents the vector of estimated parameters. The $MCWT(\hat{\Theta})$ of a single echo is given by (20) (see next page). The solution to (20) results in (21) (see next page). It is the objective of the parameter estimation algorithm to find the peaks of the TF representation of the ultrasonic echo to estimate the signal's center frequency and time-of-arrival. To accomplish this goal, the magnitude of the $MCWT(\hat{\Theta})$ is used for the TF representation of the signal, which is given by:

$$\left|MCWT(\hat{\Theta})\right| = \frac{\beta}{\sqrt{\varepsilon}}\sqrt{\frac{\pi}{\alpha+\gamma}}\exp\left[\frac{-\left(\omega_c-\frac{\omega_0}{a}\right)^2-4\alpha\gamma(b-\tau)^2}{4(\alpha+\gamma)}\right]. \quad (22)$$

The determination of the maximum of (22) can be obtained by taking partial derivatives as a function of a and b, as shown in (23) and (24) (see next page).

The maximum of (22) is reached when $b=\tau$ and $\frac{\omega_0}{a}=\omega_c$. The solutions to (23) and (24) show that the peak (maximum) of the $\left|MCWT(\hat{\Theta})\right|$ representation exactly (with no bias) estimates the time-of-arrival and center frequency of the ultrasonic echo. It is important to point out that these estimates are not a function of the phase and the bandwidth of the kernel, which is a desirable property. Consequently, the TF representation based on (22) can be obtained by using $\gamma=1$ and $\theta=0$. Furthermore, the peak value of $\left|MCWT(\hat{\Theta})\right|$ is proportional to the amplitude of the actual echo and leads to the estimation of β.

Similarly, the estimation of the phase and bandwidth factor of the ultrasonic echo is determined by taking partial derivatives of $\mathrm{Re}\left\{MCWT(\hat{\Theta})\right\}$ as a function of θ and γ, respectively. The real part of the MCWT ($\mathrm{Re}\left\{MCWT(\hat{\Theta})\right\}$) is used in this step because the phase information is not contained in the magnitude representation of the transformation shown in (25) (see next page).

The center frequency and time-of-arrival of the ultrasonic echo have been estimated already in the previous step of the parameter estimation algorithm. Hence, (25) can be simplified to:

$$\begin{aligned}\mathrm{Re}\left\{MCWT(\hat{\Theta})\right\}\Big|_{\substack{b=\tau\\ \frac{\omega_0}{a}=\omega_c}} &= \frac{\beta}{\sqrt{\varepsilon}}\sqrt{\frac{\pi}{\alpha+\gamma}}\cos(\phi-\theta)\\ &= \beta\left(\frac{2\gamma}{\pi}\right)^{1/4}\left(\frac{\pi}{\alpha+\gamma}\right)^{1/2}\\ &\quad\cdot\cos(\phi-\theta).\end{aligned} \quad (26)$$

Therefore, the partial derivatives as a function of θ and γ result in (27) and (28) (see next page). The solution to (27) leads to maximum of (26) when $\theta=\phi\pm 2\pi k$, $k=0,1,2,\ldots$. The solution to (28) results in the maximization of (26) when $\gamma=\alpha$. These results show that the $MCWT(\hat{\Theta})$ cannot only estimate the time-of-arrival and center frequency with no bias, but it also can allow the exact estimation of the phase and the bandwidth factor of the ultrasonic echo.

$$\delta_+ = \frac{-\omega_0\left(a^2\alpha+\gamma_0\right)+\sqrt{\omega_0^2\left(a^4\alpha^2+2a^2\alpha\gamma_0+\gamma_0^2\right)-4\gamma_0\left(a^4\alpha^2-\gamma_0^2\right)}}{2a\gamma_0}=0, \tag{17}$$

and

$$\delta_- = \frac{-\omega_0\left(a^2\alpha+\gamma_0\right)-\sqrt{\omega_0^2\left(a^4\alpha^2+2a^2\alpha\gamma_0+\gamma_0^2\right)-4\gamma_0\left(a^4\alpha^2-\gamma_0^2\right)}}{2a\gamma_0}=-2\omega_0. \tag{18}$$

$$\begin{aligned} MCWT(\hat{\Theta}) &= \int_{t=-\infty}^{\infty} f_\Theta(t)\psi^*_{\hat{\Theta}}(t)dt \\ &= \frac{\beta}{\sqrt{\varepsilon}}\int_{t=-\infty}^{\infty}\exp\left[-t^2(\alpha+\gamma)-t\left(-2\tau\alpha-i\omega_c-2b\gamma+\frac{i\omega_0}{a}\right)-\left(\alpha\tau^2+i\omega_c\tau-i\phi+\gamma b^2-\frac{ib\omega_0}{a}+i\theta\right)\right]dt. \end{aligned} \tag{20}$$

$$MCWT(\hat{\Theta}) = \frac{\beta}{\sqrt{\varepsilon}}\sqrt{\frac{\pi}{\alpha+\gamma}}\exp\left[\frac{-\left(\omega_c-\frac{\omega_0}{a}\right)^2-4\alpha\gamma(b-\tau)^2+i\left[4\left(\frac{\alpha\omega_0}{a}+\gamma\omega_c\right)(b-\tau)+4(\alpha+\gamma)(\phi-\theta)\right]}{4(\alpha+\gamma)}\right]. \tag{21}$$

$$\frac{\partial\left|MCWT(\hat{\Theta})\right|}{\partial a} = \frac{\beta}{\sqrt{\varepsilon}}\sqrt{\frac{\pi}{\alpha+\gamma}}\exp\left[\frac{-\left(\omega_c-\frac{\omega_0}{a}\right)^2-4\alpha\gamma(b-\tau)^2}{4(\alpha+\gamma)}\right]\left(\frac{\omega_0\left(\frac{\omega_0}{a}-\omega_c\right)}{2a^2(\alpha+\gamma)}\right)=0, \tag{23}$$

$$\frac{\partial\left|MCWT(\hat{\Theta})\right|}{\partial b} = \frac{-\beta}{\sqrt{\varepsilon}}\sqrt{\frac{\pi}{\alpha+\gamma}}\exp\left[\frac{-\left(\omega_c-\frac{\omega_0}{a}\right)^2-4\alpha\gamma(b-\tau)^2}{4(\alpha+\gamma)}\right]\left(\frac{2\alpha\gamma(b-\tau)}{(\alpha+\gamma)}\right)=0, \tag{24}$$

$$\mathrm{Re}\left\{MCWT(\hat{\Theta})\right\} = \frac{\beta}{\sqrt{\varepsilon}}\sqrt{\frac{\pi}{\alpha+\gamma}}\exp\left[\frac{-\left(\omega_c-\frac{\omega_0}{a}\right)^2-4\alpha\gamma(b-\tau)^2}{4(\alpha+\gamma)}\right]\cos\left[\frac{\left(\frac{\alpha\omega_0}{a}+\gamma\omega_c\right)(b-\tau)+(\alpha+\gamma)(\phi-\theta)}{(\alpha+\gamma)}\right]. \tag{25}$$

$$\frac{\partial\,\mathrm{Re}\left\{MCWT(\hat{\Theta})\right\}\Big|_{\substack{b=\tau\\ \frac{\omega_0}{a}=\omega_c}}}{\partial\theta} = \beta\left(\frac{2\gamma}{\pi}\right)^{1/4}\left(\frac{\pi}{\alpha+\gamma}\right)^{1/2}\sin(\phi-\theta)=0, \tag{27}$$

$$\frac{\partial\,\mathrm{Re}\left\{MCWT(\hat{\Theta})\right\}\Big|_{\substack{b=\tau\\ \frac{\omega_0}{a}=\omega_c}}}{\partial\gamma} = \frac{\beta}{2}\cos(\phi-\theta)(2\pi)^{1/4}\left(\frac{\gamma^{1/2}}{\alpha+\gamma}\right)^{-1/2}\left[\frac{(\alpha-\gamma)\gamma^{-1/2}}{2(\alpha+\gamma)^2}\right]=0. \tag{28}$$

$$s_\Theta(t)=\sum_{j=0}^{N-1}f_{\Theta j}(t)=\sum_{j=0}^{N-1}\beta_j\exp\left[-\alpha_j\left(t-\tau_j\right)^2\right]\cos\left(2\pi f_{cj}\left(t-\tau_j\right)+\phi_j\right). \tag{29}$$

B. Description of the Algorithm and Results

The successive parameter estimation technique can be applied to ultrasonic signals consisting of multiple echoes as shown in (29) (see previous page).

To search for an optimal result, the estimation method is iterated one echo at a time until the reconstruction error, E_r, is below an acceptable value $E_{\min}$. The value of $E_{\min}$ is application specific because it varies based on the requirements of the reconstruction quality of the signal. The noise level of the input signal also influences in the determination of $E_{\min}$, as the algorithm starts reconstructing noise after a certain number of iterations. If the error is not acceptable, the estimated echoes are subtracted from the original signal, and the estimation process is repeated for additional echoes until the error is within the acceptance level. If the total number of echoes N in the ultrasonic signal is unknown, then the reconstruction error is caused by two components. The first component is the error due to the incorrect estimation of the parameters for the first M echoes ($M < N$). The second error component is due to the energy of the echoes that are not estimated ($N - M$ echoes). If the signal has poor SNR, after a number of iterations the algorithm will start to track the noise instead of the ultrasonic echoes. For this reason, in a noisy environment the number of iterations should be limited. A block diagram summarizing the successive parameter estimation algorithm is shown in Fig. 2.

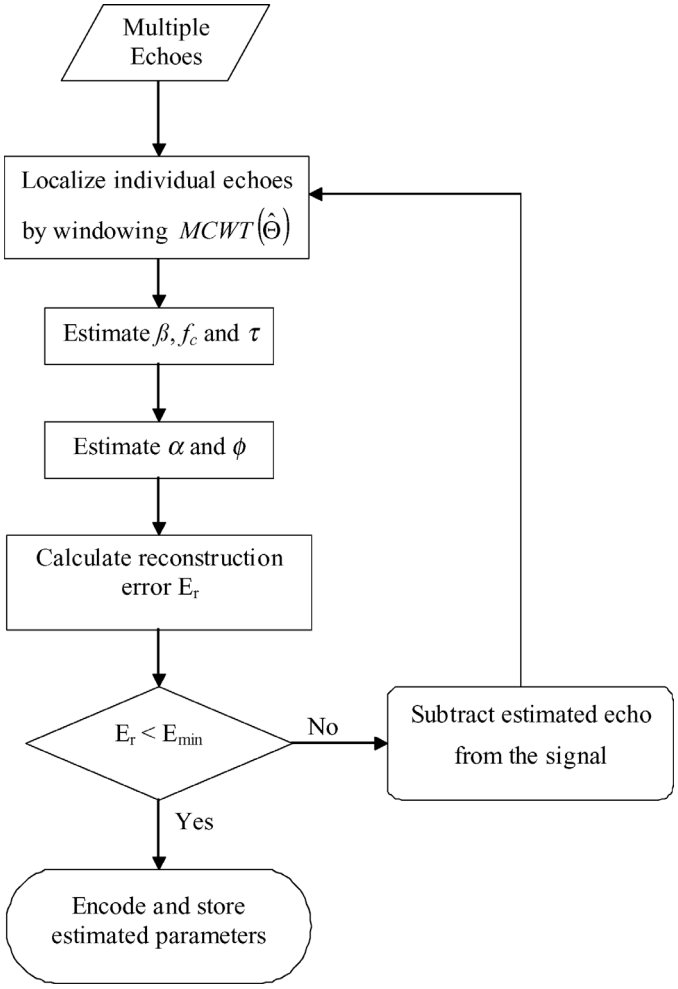

Fig. 2. Successive parameter estimation flowchart.

An example of a simulated ultrasonic echo is shown in Fig. 3(a) with a bandwidth factor $\alpha = 6$ (MHz)^2, arrival time $\tau = 3.5$ μs, center frequency $f_c = 4$ MHz, phase $\phi = 0.6$ rad, and amplitude $\beta = 1$ (i.e., $\Theta = [6,\ 1,\ 4,\ 0.6,\ 3.5]$). Both original and reconstructed signals are superimposed in Fig. 3, showing that the signal parameters are estimated as $\hat{\Theta} = [6,\ 1,\ 4,\ 0.6,\ 3.5]$ with a SNR above 200 dB, which is within the margin of computational error. Fig. 3(b) shows the TF representation ($|MCWT(\hat{\Theta})|$) of the signal shown in Fig. 3(a). Because there is only one echo in the signal, the window spans the whole signal. The peak in Fig. 3(a) coincides with the correct values for the center frequency and time-of-arrival (f_c and τ) of the echo. Fig. 3(c) shows the representation of $\mathrm{Re}\left\{MCWT(\hat{\Theta})\right\}$ as a function of bandwidth and phase. The results in Fig. 3(c) show that the peaks are located at the correct values of the phase and bandwidth (ϕ and α) of the echo.

Fig. 3 shows that the estimation of a noise-free single echo is exact. This ideal situation is not encountered in many practical applications. Moreover, it is important to point out that the parameter estimation efficiency is degraded in a noisy environment. One also would expect that the degree of degradation depends on the input SNR, where $SNR = 10 \log \frac{P_{signal}}{P_{noise}}$, and P_{signal} and P_{noise} represent the power of the signal and the power of the noise, respectively. We have examined the performance of the parameter estimation algorithm by evaluating the SNR enhancement (i.e., the difference between the output SNR and the input SNR). Fig. 4 shows the output SNR as a function of the input SNR. Each point in this plot represents a realization of the noise with different energies added to the single echo, and the respective output SNR represents the improvement achieved by the parameter estimation algorithm. The parameters of the single echo were not changed. The input SNR has been varied from -12 dB (severely poor SNR) to 36 dB (high SNR). It has been observed that the SNR enhancement is well above 10 dB, and enhancements as high as 60 dB can be achieved. These results clearly indicate that the successive parameter estimation algorithm is robust and performs well. Fig. 5 shows two examples of echoes with an input SNR of -2 dB (moderately poor SNR) and -12 dB (severely poor SNR). In both cases the estimated echoes are closely matched to the actual echo [see Figs. 5(b) and (f)]. The estimated echoes show a SNR enhancement of above 25 dB.

The performance of the parameter estimation algorithm is also expected to degrade in an environment with multiple interfering echoes. The following example illustrates the performance of the algorithm when applied to two highly interfering echoes. The TF representation of the two interfering echoes is shown in Fig. 6(a). The procedure used to design the window is based on the determination of the peaks and valleys of the MCWT representation of the

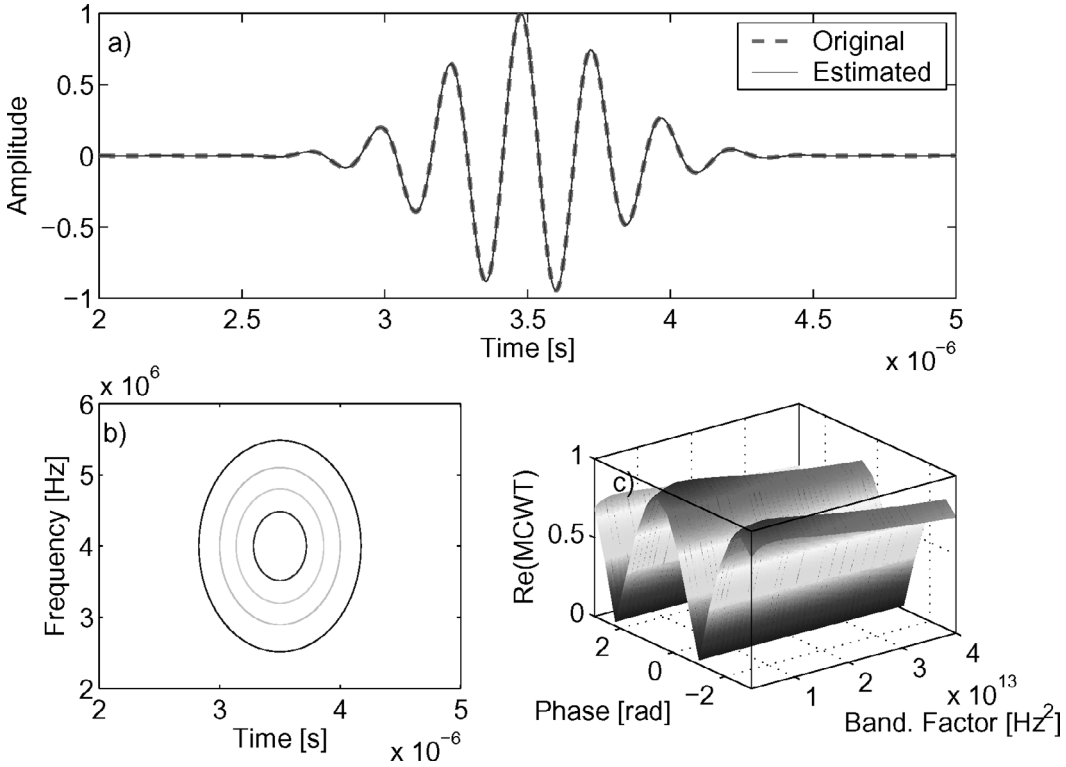

Fig. 3. (a) Original signal (dashed line, $\Theta = [6,\ 1,\ 4,\ 0.6,\ 3.5]$), estimated signal (solid line, $\hat{\Theta} = [6,\ 1,\ 4,\ 0.6,\ 3.5]$). (b) Time × frequency representation of signal in (a). (c) Phase × bandwidth representation of signal in (a).

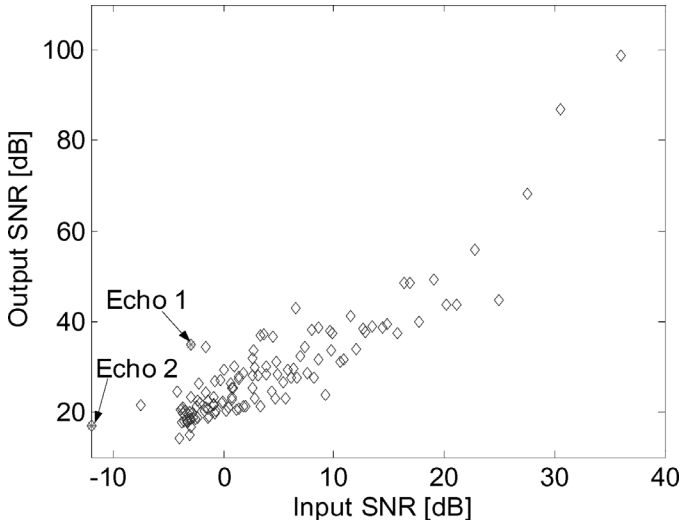

Fig. 4. Input and output SNRs.

ultrasonic signal. Once the peaks are found, the boundaries of the window are determined by the valleys between peaks. An automatic algorithm uses the projection of the MCWT in the frequency domain [Fig. 6(b)] and in the time domain [Fig. 6(c)] to localize the peaks and valleys of the TF representation. If more than two peaks are found, the window for each echo is constructed by the intersection of such boundaries. In noisy environments, it is important to constrain the size of the window in order to limit the amount of noise into the signal estimation step. But it also is important to keep as much of the signal information as possible. Hence, the boundaries in the TF representation may not truthfully characterize the location of the echoes. For this reason, the width of the window can be set to a predetermined value that may depend on the noise level, bandwidth, and energy of the echo. These are the tradeoffs one must take in consideration when designing the TF windowing algorithm.

The actual and estimated parameters are presented in Table I. The estimated echoes are superimposed to the original signal in Fig. 7, in which the SNR of the estimated echoes is better than 20 dB. From Fig. 7 one can conclude that the successive parameter estimation algorithm is successful, even in a situation in which multiple echoes interfere in both time and frequency.

III. Performance Evaluation with Simulated and Experimental Ultrasonic Signals

In this section we analyze the performance of the successive parameter estimation method using composite and highly interfering simulated (see Figs. 8–10) and experimental (see Fig. 11) echoes. Fig. 8(a) shows the time-domain representation of a simulated ultrasonic signal with 10 interfering echoes. White noise was added to this signal, and the result is shown in Fig. 8(c), in which the SNR is 1.5 dB. The SNR of the estimated signal as shown in Fig. 8(e) is 14 dB. The actual [see Fig. 8(b)] and the estimated [see Fig. 8(f)] TF representations of this composite signal are also closely matched.

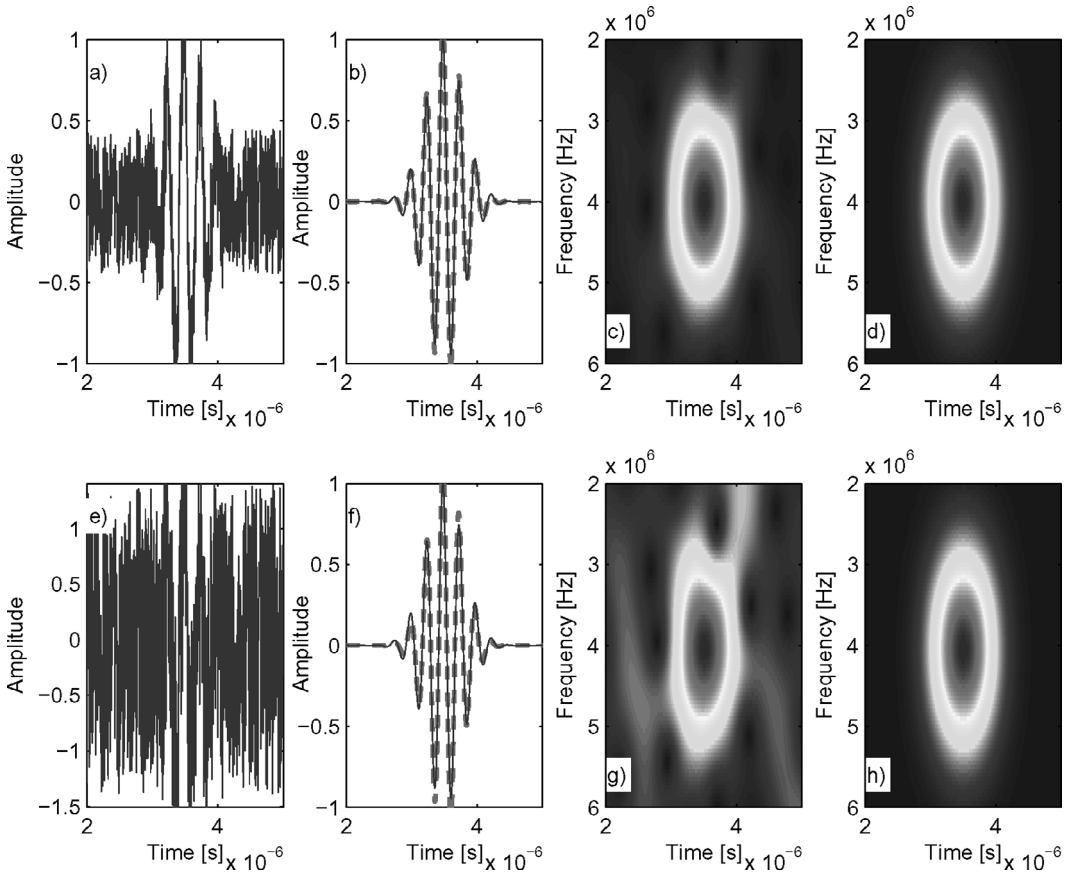

Fig. 5. (a) Echo 1 with moderately poor SNR. (b) Estimated Echo 1 superimposed with actual echo. (c) TF representation of Echo 1. (d) TF representation of estimated Echo 1. (e) Echo 2 with severely poor SNR. (f) Estimated Echo 2 superimposed with actual echo. (g) TF representation of Echo 2. (h) TF representation of estimated Echo 2.

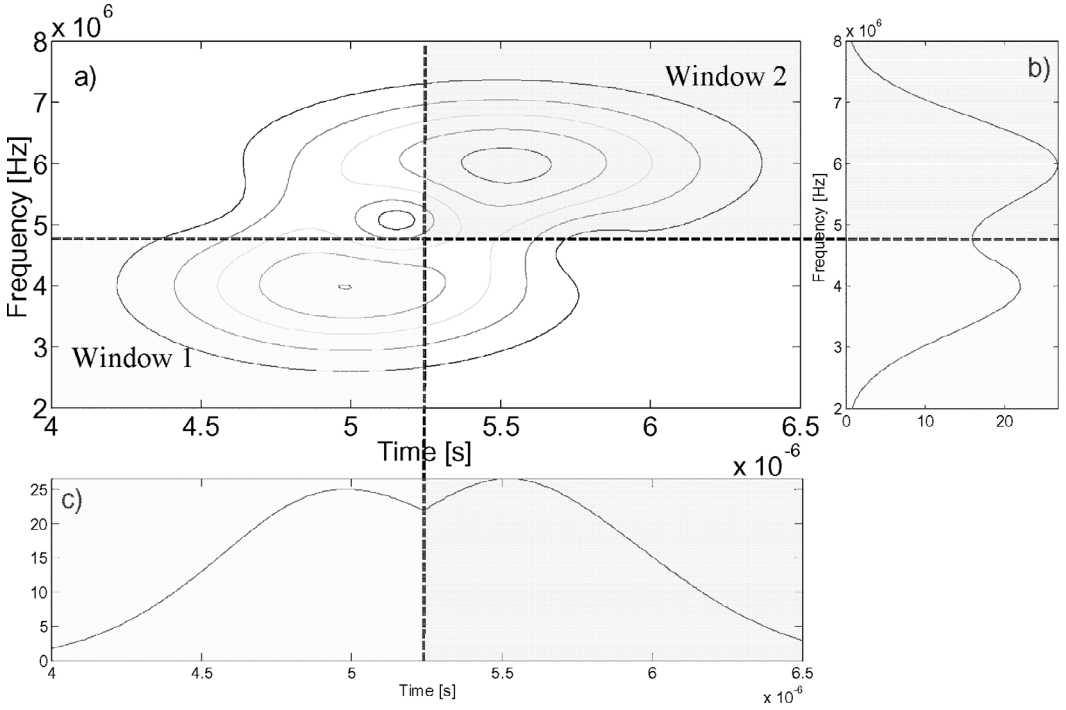

Fig. 6. (a) TF representation of two interfering echoes. (b) Projection in the frequency domain. (c) Projection in the time domain.

TABLE I
TWO INTERFERING ECHOES, ORIGINAL AND ESTIMATED PARAMETERS.

Echo	f [MHz]	$\hat{f}$ [MHz]	τ [μs]	$\hat{\tau}$ [μs]	α [MHz]^2	$\hat{\alpha}$ [MHz]^2	β	$\hat{\beta}$	ϕ [rad]	$\hat{\phi}$ [rad]
First	4	4	5	5	4	4.1	1	0.997	0	0
Second	6	5.95	5.5	5.52	3	3	1	1.1032	1	1.8

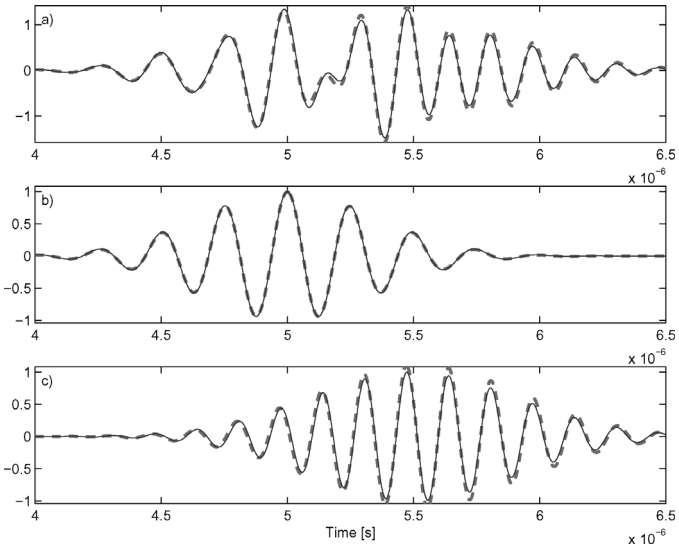

Fig. 7. Original (solid line) and estimated (dashed line) signals. (a) Two interfering echoes. (b) First echo. (c) Second echo.

Fig. 9 shows the sequence of estimated single echoes out of the 10 interfering echoes in Fig. 8. The original and estimated single echoes are superimposed in Fig. 9. Because this is a successive parameter estimation algorithm, the echoes with the highest energy in the TF domain are estimated first. The original signal parameters, Θ, as well as the estimated parameters, $\hat{\Theta}$, are shown in Table II. Both Table II and Fig. 9 confirm the successive parameter estimation algorithm effectiveness in estimating parameters with a high level of accuracy.

The successive estimation of the ultrasonic echoes is terminated once the energy of the last estimated echo was 20 dB below the energy of the most dominating echo. The clutter and thermal noise vary in different applications; hence, the threshold used in the algorithm must change accordingly. The 20 dB threshold is specific to this example. If the algorithm continues after this point, it begins to estimate low intensity clutter and measurement noise. Fig. 10 shows the succession of the algorithm in estimating from the most dominant echo in the signal to the least dominant echo.

The parameter-estimation method provides a high level of data compression while maintaining a high-fidelity representation of the signal. The successive parameter estimation algorithm achieves a data compression ratio given by:

$$CR = 1 - \frac{5N}{J}, \tag{30}$$

where J is the number of samples and N is the number of echoes in the ultrasonic signal with five estimated parameters per single echo. The original signal [see Fig. 8(a)] has 2048, 16-bit coefficients, and the estimated signal can be reconstructed with 50, 16-bit coefficients. Hence, the algorithm achieved a data compression ratio of 97%. Further compression can be achieved by encoding the estimated parameters using lossless compression algorithms [23] and [24]. The successive parameter estimation algorithm can also iterate for more than 10 echoes to improve the SNR of the original signal even further. Fig. 12 shows the SNR and compression ratio for 50 iterations of the algorithm. It can be observed that, during the first 18 iterations (from CR = 0.99 to CR = 0.96), the SNR is improved from 0 dB to 20 dB. After this point, the algorithm proceeds estimating noise instead of the original echoes, which leads to a decrease in the SNR. Furthermore, the SNR improvement reaches a plateau of about 19 dB beyond 25 echo estimations. In summary, the algorithm is robust in the estimation of echoes in an ultrasonic signal embedded in noise. Nevertheless, the successive parameter estimation algorithm achieves a high rate of data compression if the signal has a limited number of echoes. In the case in which the signal contains a very large number of multiple interfering echoes [30] the performance of data compression may deteriorate.

The parameter estimation algorithm also was evaluated using an ultrasonic experimental signal consisting of multiple interfering echoes. Fig. 11(a) shows an experimental signal acquired from a steel sample block with a flat-bottom hole using a 5 MHz transducer and sampling rate of 100 MHz. The experimental signal has a very poor SNR and the flaw echo shows interference from microstructure scattering and measurement noise. Fig. 11(c) shows the estimated signal that has been successful in filtering out the noise and achieving an accurate estimation of the flaw echo using 20 echoes. The TF representation of the experimental and estimated signals is shown in Figs. 11(b) and (d), respectively. Fig. 11 clearly shows that the dominant flaw echo has lower frequency content when compared to the backscattered grain echoes [31].

IV. CONCLUSIONS

In this study, we have analyzed a signal modeling and successive parameter estimation technique to compress and denoise ultrasonic signals. It has been shown analytically that the CWT leads to an exact estimation of the time-of-arrival and a biased estimation of the center

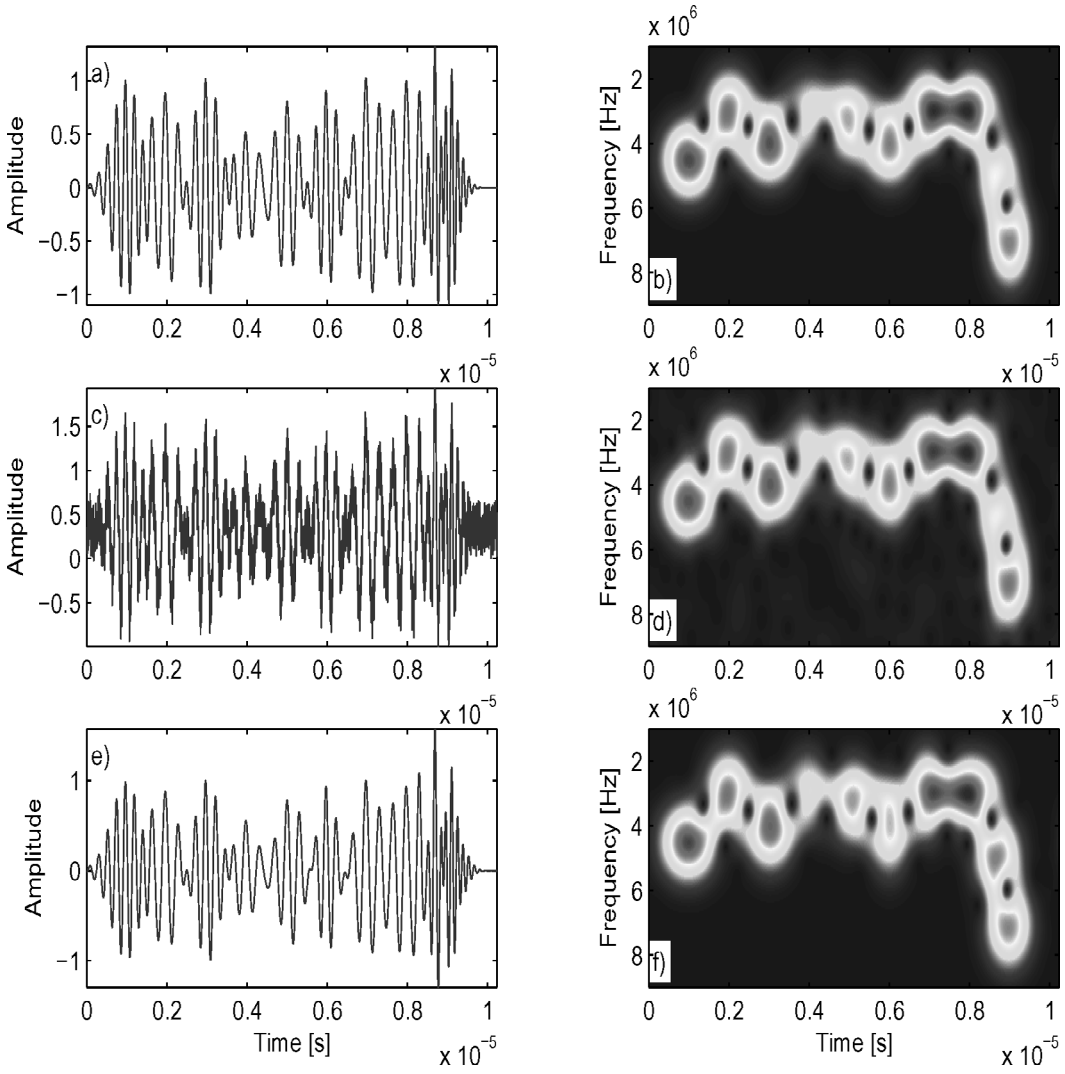

Fig. 8. (a) Original signal. (b) TF representation of signal in (a). (c) Original signal corrupted with noise. (d) TF representation of signal in (c). (e) Estimated signal. (f) TF representation of signal in (e).

TABLE II
ORIGINAL AND ESTIMATED PARAMETERS OF MULTIPLE INTERFERING SIMULATED ECHOES.

Echo	f [MHz]	$\hat{f}$ [MHz]	τ [μs]	$\hat{\tau}$ [μs]	α [MHz]^2	$\hat{\alpha}$ [MHz]^2	β	$\hat{\beta}$	ϕ [rad]	$\hat{\phi}$ [rad]
a	4.5	4.5000	1	0.986	4	3.6000	1	0.9835	1	0.6000
b	4	3.9500	6	5.997	4.8	9.7000	0.9	0.9273	0.8	0.7000
c	4	4.0000	3	3.019	4	5.6000	1	0.9983	0.9	1.4000
d	7	7.1000	9	8.980	8	6.0000	1	0.9120	1.5	0.6000
e	3	3.0000	2	1.975	5	5.8000	0.9	0.9133	0.8	0.3000
f	5	4.9500	8.7	8.692	8	5.8000	0.8	0.9062	0.2	0
g	3.3	3.2500	5	5.094	5	5.4000	0.8	0.7849	0	2.0000
h	3	3.0000	7	0.6963	5	7.6000	1	0.9101	0.7	0
i	3	3.000	8	8.077	4	2.0000	1	1.0541	0.5	2.0000
j	3	2.9500	4	3.970	4	6.2000	0.5	0.5504	0.7	0

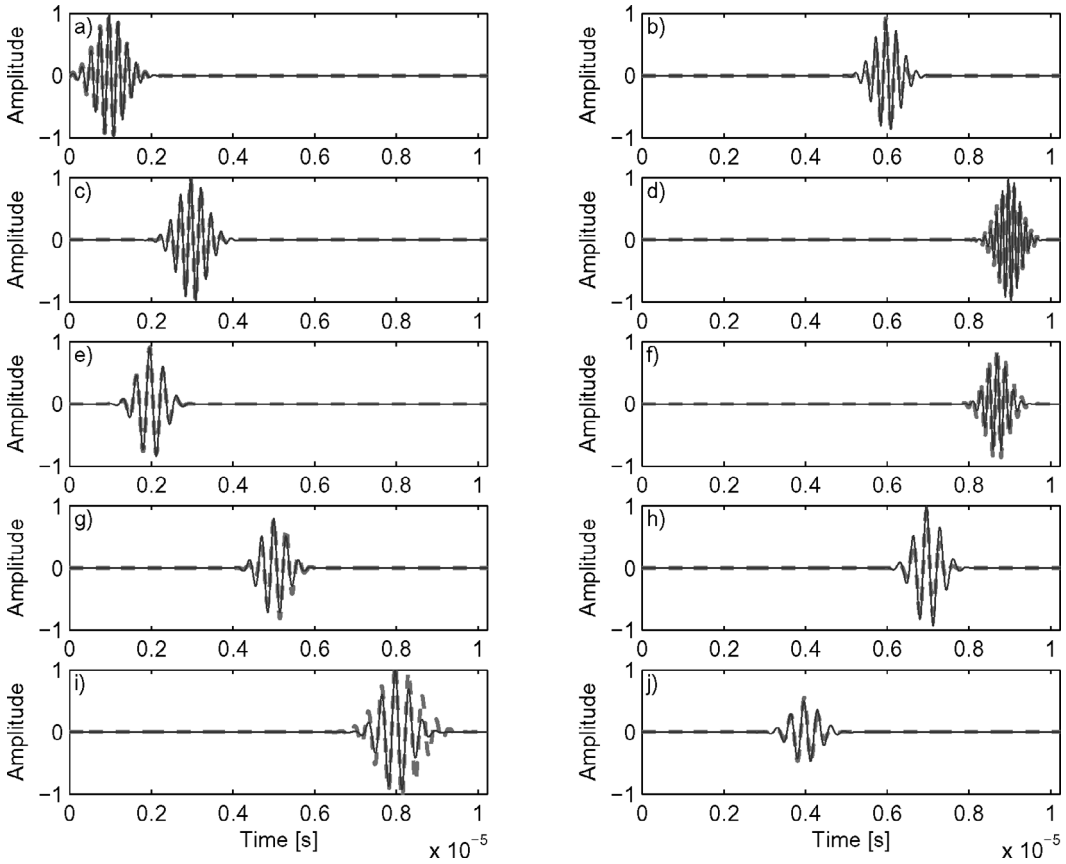

Fig. 9. Sequence of single echo estimations from highest energy echo shown in (a) to the lowest energy echo shown in (j) superimposed with the original echoes. The solid line represents the original echoes, and the dashed line represents the estimated echoes.

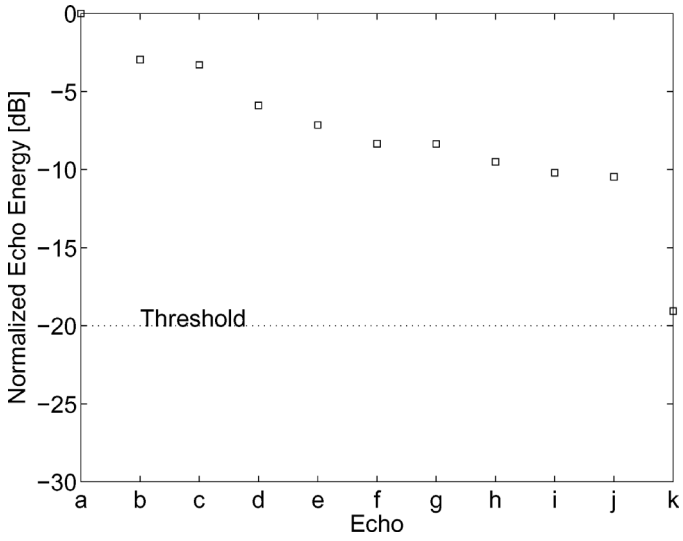

Fig. 10. Energy of estimated echoes from the highest energy to the lowest energy.

frequency. Consequently, a MCWT based on the Gabor-Helstrom transform has been introduced to estimate both the time-of-arrival and the center frequency of ultrasonic echoes exactly. The parameter estimation algorithm uses an overcomplete Morlet wavelet kernel for estimating all of the ultrasonic echo parameters. It has been shown through computer simulations and analytical derivations that the MCWT algorithm can efficiently estimate all the echo parameters.

The parameters of the ultrasonic echo affect the overall estimation error differently. Thus, we have analyzed the sensitivity of the reconstruction error to the variation of the estimated parameters. The results presented reveal that center frequency and time-of-arrival are the most critical parameters in the estimation of ultrasonic echoes. These parameters are estimated directly from the peaks in the TF representation of the signal.

The successive parameter estimation algorithm relies on an automatic windowing procedure to find and localize single echoes in the signal's TF representation. This procedure uses the time and frequency domain projections of the TF representation of the signal to determine the boundaries of the window. This method is shown to be successful in high SNR environments, but its performance deteriorates as the noise level increases. To remedy this problem, a different procedure with a reduced size window is desirable for low SNR signals.

The performance of the data compression algorithm has been evaluated using both simulated and experimental ultrasonic signals. The algorithm is able to compress ultrasonic data by estimating the echo parameters with high accuracy, which leads to high fidelity signal reconstruction capabilities. The algorithm also performs well in noisy en-

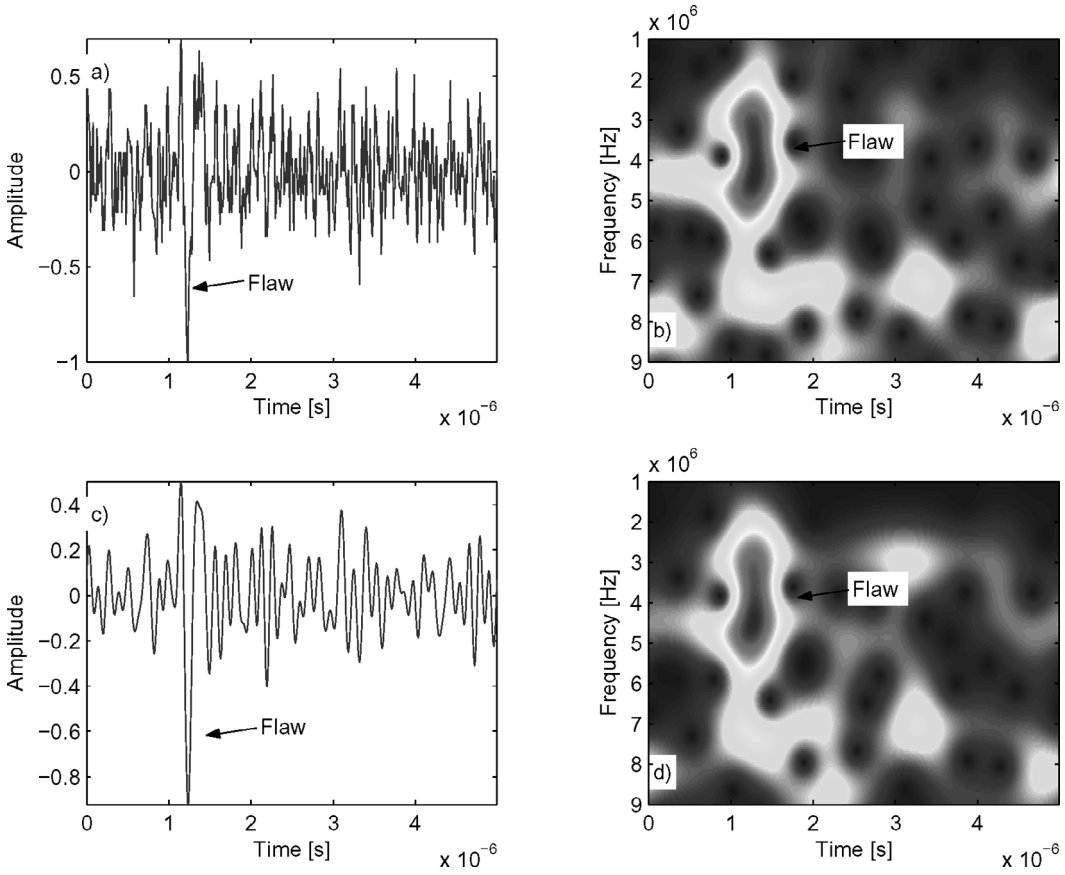

Fig. 11. (a) Experimental signal. (b) TF representation of signal in (a). (c) Estimated signal. (d) TF representation of signal in (c).

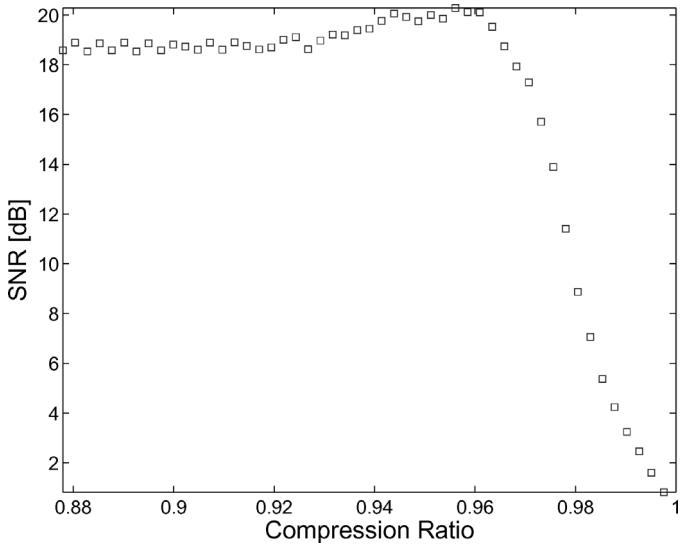

Fig. 12. SNR enhancement of successive parameter estimation algorithm as function of compression ratio.

vironments in which SNR enhancements beyond 60 dB are feasible. Overall, the signal modeling and parameter estimation algorithm presented in this paper not only offers data compression capabilities, but also provides parameters that can be used for signal deconvolution, target detection, pattern recognition, and material characterization.

References

[1] J. Saniie, "Ultrasonic signal processing: System identification and parameter estimation of reverberant and inhomogeneous targets," Ph.D. dissertation, Purdue University, West Lafayette, IN, Aug. 1981.

[2] J. Saniie, T. Wang, and N. M. Bilgutay, "Statistical evaluation of backscattered ultrasonic grain signals," *J. Acoust. Soc. Amer.*, vol. 84, pp. 400–408, July 1988.

[3] J. Saniie and D. T. Nagle, "Pattern recognition in the ultrasonic imaging of reverberant multilayered structures," *IEEE Trans. Ultrason., Ferroelect., Freq. Contr.*, vol. 36, pp. 80–92, Jan. 1989.

[4] L. L. Fellingham and F. G. Sommer, "Ultrasonic characterization of tissue structure in the in vivo human liver and spleen," *IEEE Trans. Sonics Ultrason.*, vol. SU-31, pp. 418–428, July 1984.

[5] D. L. Liu and M. Saito, "A new method for estimating the acoustic attenuation coefficient of tissue from reflected ultrasound signals," *IEEE Trans. Med. Imag.*, vol. 8, pp. 107–110, Mar. 1989.

[6] L. Landini and L. Verrazzani, "Spectral characterization of tissues microstructure by ultrasounds: A stochastic approach," *IEEE Trans. Ultrason., Ferroelect., Freq. Contr.*, vol. 37, pp. 448–456, Sep. 1990.

[7] K. A. Wear, R. F. Wagner, M. F. Insana, and T. J. Hall, "Application of autoregressive spectral analysis to cepstral estimation of mean scatterer spacing," *IEEE Trans. Ultrason., Ferroelect., Freq. Contr.*, vol. 40, pp. 50–58, Jan. 1993.

[8] E. J. Chen, W. K. Jenkins, and W. D. O'Brien, Jr., "The impact of various imaging parameters on ultrasonic displacement and velocity estimates," *IEEE Trans. Ultrason., Ferroelect., Freq. Contr.*, vol. 41, pp. 293–301, May 1994.

[9] T. Varghese and K. D. Donohue, "Estimating mean scatterer spacing with the frequency-smoothed spectral autocorrelation function," *IEEE Trans. Ultrason., Ferroelect., Freq. Contr.*, vol. 42, pp. 451–463, May 1995.

[10] C. Simon, J. Shen, R. Seip, and E. S. Ebbini, "A robust and computationally efficient algorithm for mean scatterer spacing estimation," *IEEE Trans. Ultrason., Ferroelect., Freq. Contr.*, vol. 44, pp. 882–894, July 1997.
[11] U. R. Abeyratne, A. P. Petropulu, and J. M. Reid, "On modeling the tissue response from ultrasonic B-scan images," *IEEE Trans. Med. Imag.*, vol. 15, pp. 479–490, Aug. 1996.
[12] P. Chaturvedi and M. F. Insana, "Errors in biased estimators for parametric ultrasonic imaging," *IEEE Trans. Med. Imag.*, vol. 17, pp. 53–61, Feb. 1998.
[13] M. Feder and E. Weinstein, "Parameter estimation of superimposed signals using the EM algorithm," *IEEE Trans. Acoust. Speech Signal Processing*, vol. 36, pp. 477–489, Apr. 1988.
[14] R. Demirli and J. Saniie, "Model-based estimation of ultrasonic echoes. Part I: Analysis and algorithms," *IEEE Trans. Ultrason., Ferroelect., Freq. Contr.*, vol. 48, pp. 787–802, May 2001.
[15] R. Demirli and J. Saniie, "Model-based estimation of ultrasonic echoes. Part II: Nondestructive evaluation applications," *IEEE Trans. Ultrason., Ferroelect., Freq. Contr.*, vol. 48, no. 3, pp. 803–811, May 2001.
[16] M. A. Malik, "Unified time-frequency analysis of ultrasonic signals," Ph.D. dissertation, Illinois Institute of Technology, Chicago, IL, July 1995.
[17] A. Abbate, J. Koay, J. Frankel, S. C. Schroeder, and P. Das, "Signal detection and noise suppression using a wavelet transform signal processor: Application to ultrasonic flaw detection," *IEEE Trans. Ultrason., Ferroelect., Freq. Contr.*, vol. 44, pp. 14–26, Jan. 1997.
[18] G. Cardoso and J. Saniie, "Data compression and noise suppression of ultrasonic NDE signals using wavelets," in *Proc. IEEE Ultrason. Symp.*, Oct. 2003, pp. 250–253.
[19] A. Grossmann and J. Morlet, "Decomposition of Hardy functions into square integrable wavelets of constant shape," *SIAM J. Math. Anal.*, vol. 15, pp. 723–736, 1984.
[20] P. Goupillaud, A. Grossmann, and J. Morlet, "Cycle-octave and related transforms in seismic signal analysis," *Amer. Geoexploration*, vol. 23, pp. 85–102, 1984.
[21] G. K. Wallace, "The JPEG still picture compression standard," *Commun. ACM*, vol. 34, pp. 31–44, Apr. 1991.
[22] A. Said and W. A. Pearlman, "A new fast and efficient coder based on set partitioning in hierarchical trees," *IEEE Trans. Circuits Syst. Video Technol.*, pp. 243–250, June 1996.
[23] A. Gersho and R. M. Gray, *Vector Quantization and Signal Compression*. Boston: Kluwer Academic, 1991.
[24] K. Sayood, *Introduction to Data Compression*. San Francisco: Morgan Kaufmann, 2000.
[25] G. Cardoso and J. Saniie, "Compression of ultrasonic data using transform thresholding and parameter estimation techniques," in *Proc. IEEE Ultrason. Symp.*, Oct. 2002, pp. 837–840.
[26] M. Sandell and A. Grennberg, "Estimation of the spatial impulse response of an ultrasonic transducer using a tomographic approach," *J. Acoust. Soc. Amer.*, vol. 98, pp. 2094–2103, Oct. 1995.
[27] R. M. Rao and A. S. Bopardikar, *Wavelet Transforms*. Reading, MA: Addison-Wesley, 1998.
[28] G. Cardoso and J. Saniie, "Optimal wavelet estimation for data compression and noise suppression of ultrasonic NDE signals," in *Proc. IEEE Ultrason. Symp.*, Oct. 2001, pp. 675–678.
[29] C. W. Helstrom, "An expansion of a signal in Gaussian elementary signals," *IEEE Trans. Inform. Theory*, vol. 12, pp. 81–82, Jan. 1966.
[30] J. A. Jensen and S. I. Nikolov, "Fast simulation of ultrasound images," in *Proc. IEEE Ultrason. Symp.*, Oct. 2000, pp. 1721–1724.
[31] J. Saniie and D. T. Nagle, "Analysis of order-statistic CFAR threshold estimators for improved ultrasonic flaw detection," *IEEE Trans. Ultrason., Ferroelect., Freq. Contr.*, vol. 39, pp. 618–630, Sep. 1992.

Guilherme Cardoso was born in Porto Alegre, Brazil, on April 27, 1976. He received his B.S. degree in electrical engineering from the Federal University of Rio Grande do Sul, Porto Alegre, Rio Grande do Sul, Brazil, and his M.S.E.E. degree from the Illinois Institute of Technology (IIT), Chicago, IL, in 1998 and 2000, respectively. Since 1998 he has been working at Fermi National Accelerator Laboratory (Fermilab), Batavia, IL, in the research and development of multichip modules and electronics for tracking detectors for high energy physics experiments. He is currently pursuing a Ph.D. degree in electrical engineering at IIT researching subband and transforms coding techniques for signal processing and data compression.

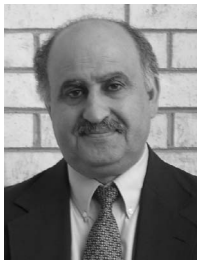

Jafar Saniie (S'80–M'81–M'83–SM'91) was born in Iran on March 21, 1952. He received his B.S. degree in electrical engineering from the University of Maryland, College Park, MD, in 1974. He received his M.S. degree in biomedical engineering in 1977 from Case Western Reserve University, Cleveland, OH, and his Ph.D. degree in electrical engineering in 1981 from Purdue University, West Lafayette, IN. In 1981 Dr. Saniie joined the Department of Applied Physics, University of Helsinki, Finland, to conduct research in Photothermal and Photoacoustic Imaging. Since 1983 he has been with the Department of Electrical and Computer Engineering at Illinois Institute of Technology, Chicago, IL, where he is a Professor, Director of the Ultrasonic Information Processing Laboratory, and Director of Graduate and Computer Engineering.

Dr. Saniie's research interests and activities are in ultrasonic signal and image processing, statistical pattern recognition, estimation and detection, embedded digital systems, digital signal processing with field programmable gate arrays, and ultrasonic nondestructive testing and imaging. In particular, he has performed extensive work in the areas of frequency diverse ultrasonic flaw enhancement techniques, embedded signal processing architectures for ultrasonic imaging, ultrasonic data compression, nonlinear signal processing in target detection, ultrasonic imaging of reverberant multilayer structures, morphological processing and pattern recognition in ultrasonic imaging, time-frequency analysis of ultrasonic signals, and application of neural networks for detecting flaw echoes and classifying microstructural scattering.

Dr. Saniie has been a Technical Committee Member of the IEEE Ultrasonics Symposium since 1987 (currently he is the chair of Sensors, NDE & Industrial Applications), Associate Editor of the *IEEE Transactions on Ultrasonics, Ferroelectrics, and Frequency Control* since 1994, Program Coordinator and Local Chair of the Conference on Properties and Applications of Magnetic Materials since 1985, and Editorial Advisory member of the *Nondestructive Testing and Evaluation Journal* (1986–1996). He is a member of Sigma Xi, IEEE, Tau Beta Pi, Eta Kappa Nu, and has been the IEEE Branch Counselor (1983–1990). He is the 1986 recipient of the Outstanding IEEE Student Counselor Award.